A second order finite-volume scheme on cartesian grids for Euler equations

Lisl Weynans, Yannick Gorsse, Angelo Iollo

Joint EUROMECH / ERCOFTAC Colloquium 549
"Immersed Boundary Methods: Current Status and Future Research Directions"
Leiden, The Netherlands, 17-19 June 2013

A second order finite-volume scheme on cartesian grids for Euler equations

L. Weynans[1], Y. Gorsse[2] and A. Iollo[1]

[1] Univ. Bordeaux, CNRS and INRIA, IMB, UMR5251, F-33400, Talence, France
lisl.weynans@math.u-bordeaux1.fr

[2] CEA Cadarache, France

ABSTRACT

We present a simple globally second order scheme inspired by ghost cell approaches to solve compressible inviscid flows [4]. In the fluid domain, away from the boundary, we use a classical finite-volume method based on an approximate Riemann solver for the convective fluxes. At the cells located on the boundary, we solve an *ad hoc* Riemann problem taking into account the relevant boundary condition for the convective fluxes by an appropriate definition of the contact discontinuity speed. To avoid pressure oscillations near the solid we balance the boundary condition with an extrapolation of the fluid values, as a function of the angle between the normal to the solid and the normal to the cell. Our objective is to device a method that can easily be implemented in existing codes and that is suitable for massive parallelization.

1. Resolution in the fluid domain

1.1 Governing equations

The compressible Euler equations are:

$$\frac{\partial \rho}{\partial t} + \nabla \cdot \rho \mathbf{u} = 0 \tag{1}$$

$$\frac{\partial \rho \mathbf{u}}{\partial t} + \nabla \cdot (\rho \mathbf{u} \otimes \mathbf{u} + p\mathbf{n}) = 0 \tag{2}$$

$$\frac{\partial E}{\partial t} + \nabla \cdot ((E+p)\mathbf{u}) = 0 \tag{3}$$

$$\tag{4}$$

where E denotes the total energy per unit volume. For a perfect gas

$$E = \frac{p}{\gamma - 1} + \frac{1}{2}\rho \mathbf{u}^2 \text{ and } p = \rho RT \tag{5}$$

1.2 Discretization far in the fluid domain and boundary representation

We focus on a two-dimensional setting. We consider a cartesian grid, with indexes i and j and spacings h_x and h_y in the x and y direction, respectively. Far from the boundary with the solid, we use a classical finite-volume scheme based on an approximate Riemann solver, and a second-order Runge-Kutta scheme for the time integration.

In order to improve accuracy at the solid walls crossing the grid cells we need additional geometric information. This information, mainly the distance from the wall and the wall normal, is provided by the distance function. The level set method, introduced by Osher and Sethian is used to implicitly represent the interface of solid in the computational domain. The zero isoline of the level set function represents the boundary Σ of the immersed body. The level set function is defined here by:

$$\varphi(x) = \begin{cases} dist_\Sigma(x) & \text{outside of the solid} \\ -dist_\Sigma(x) & \text{inside of the solid} \end{cases} \tag{6}$$

A useful property of this level set function is:

$$\mathbf{n}(x) = \nabla \varphi(x) \tag{7}$$

where $\mathbf{n}(x)$ is the outward normal vector of the isoline of ϕ passing on x. In particular, this allows to compute the values of the normal to the interface, represented by the isoline $\varphi = 0$.

2. A second order impermeability condition

The boundary condition that we have to impose is $\mathbf{u}_A.\mathbf{n}_A = 0$, where $\mathbf{u}_A$ is the speed of the fluid at the boundary, and $\mathbf{n}_A$ the outward normal vector of the body. We want to impose the boundary condition on what we call the interface points: the intersections between the interface ($\varphi = 0$) and the segment connecting the two cell centers concerned by the sign change (for example the points A, B and C on Fig. 1(a)). To this purpose, a fictitious state is created for instance between the cells (i, j) and $(i+1, j)$ on Fig. 1(a).

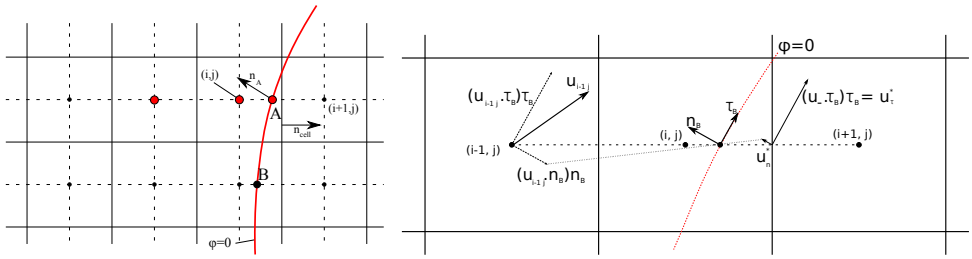

(a) Geometric configuration (b) Construction of vector

Figure 1: Fig. 1(a): Example of geometric configuration at the interface. A is the interface point located between (i, j) and $(i+1, j)$. The flux on cell interface $(i+1/2, j)$ is modified to enforce the boundary condition on A. Fig. 1(b): Graphical illustration of the construction of the $\mathbf{u}^*$ vector.

According to Fig. 1(b) and considering the $(i+1/2, j)$-flux, we compute the left state primitive variables u_-, p_-, c_- relative to the Riemann problem at the concerned numerical interface by a standard MUSCL reconstruction. The left state will be and $U_- = (u_-, v_w, p_-, c_-)$ and the right state $U_+ = (-u_- + 2u_w, v_w, p_w, c_w)$, where:

- $\begin{pmatrix} u_w \\ v_w \\ p_w \\ c_w \end{pmatrix} = \alpha \begin{pmatrix} u^* \\ v^* \\ p_- \\ c_- \end{pmatrix} + (1-\alpha) \begin{pmatrix} u_f \\ v_f \\ p_f \\ c_f \end{pmatrix}$;
- $\alpha = \mathbf{n}_A.\mathbf{n}_{cell}$;
- (u_f, v_f, p_f, c_f) is computed as a linear extrapolation of the fluid variables to the point $x_{i+1/2\,j}$ using the variables and the slopes of the closest upstream fluid cell. It plays a role when the scalar product between the normal to the physical boundary and the normal to the mesh side is close to zero, because in this case the boundary condition only weakly affects the numerical flux.

We determine the value of the contact discontinuity speed $\mathbf{u}^*$, relative to a Riemann problem defined in the direction normal to the cell side through $x_{i+1/2,j}$, consistent at second order accuracy with $\mathbf{u}_A \cdot \mathbf{n}_A = 0$ in A. The vector $\mathbf{u}^*$ is determined as follows:

$$\left.\begin{array}{l} \mathbf{u}^*.\mathbf{n}_A = u_n^* = \mathbf{u}_A.\mathbf{n}_A + \left(\frac{1}{2} - d\right) s_A^{\mathbf{n}} \\ \mathbf{u}^*.\tau_A = u_\tau^* = \mathbf{u}_-.\tau_A \end{array}\right\} \Rightarrow \mathbf{u}^* = \begin{pmatrix} u_n^* n_x + u_\tau^* \tau_x \\ u_n^* n_y + u_\tau^* \tau_y \end{pmatrix}$$

Where $\mathbf{u}_A$ is the velocity of the obstacle ($= 0$ for a steady body), $\mathbf{n}_A = \left(n_x, n_y\right)^t$ and $\tau_A = \left(\tau_x, \tau_y\right)^t$ are respectively the normal and tangential vectors to the boundary at point A and the slope $s_A^{\mathbf{n}}$ is defined as:

$$s_A^{\mathbf{n}} = \mathbf{u}_A.\mathbf{n}_A - \mathbf{u}_i.\mathbf{n}_A + \frac{1-d}{1+d}\left(\mathbf{u}_A.\mathbf{n}_A - \mathbf{u}_{i-1}.\mathbf{n}_A\right). \tag{8}$$

3. Numerical illustrations

The Ringleb flow

The Ringleb flow refers to an exact solution of Euler equations. The solution is obtained with the hodograph method. In our test case, the computational domain is $[-0.5; -0.1] \times [0; 0.6]$ and we numerically solve the flow between the streamlines $\Psi_1 = 0.8$ and $\Psi_2 = 0.9$. The inlet and outlet boundary condition are supersonic for $y = 0$ and $y = 0.6$ respectively.

The convergence orders are calculated in L_2 norm on four different grids 32×48, 64×96, 128×192 and 256×384. The results for the L_2 norm of our method are compared to a simple symmetry technique, the ghost-cell CCST method [3], that relies on a local isoentropic flow model at the wall, and a standard finite-volume scheme case with a body-fitted meshs in Fig. 2.

The overall results show that the classical symmetry scheme is first order accurate in the L_2 norm. The other schemes have overall comparable accuracy, although the amplitude of the error is lower for the present scheme compared to the ghost-cell CCST method. For the same test case, Coirier and Powell [1] observed also a convergence order between one and two in the case of their own cartesian method.

Mach 10 shock over three spheres

The computation of a planar shock reflecting over three spheres is performed. The spheres are located at (0,0,0), (-0.75, 1.4,-1.4),

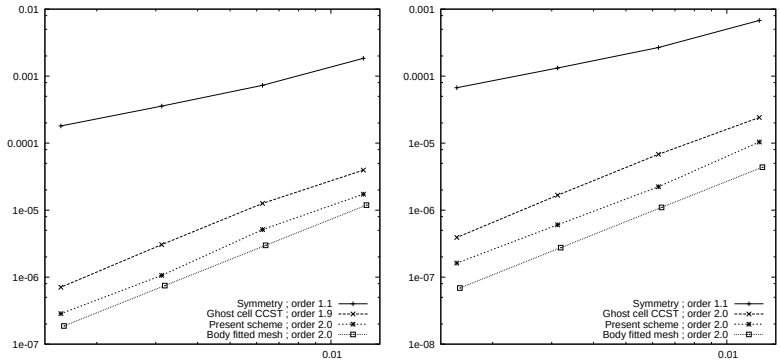

(a) Pressure (b) Sound speed

Figure 2: Comparison of the L_2 accuracy of the present scheme with several methods. The convergence orders are detailed in the legend.

(0,-2,0) with radii 1, 0.4, 0.3, respectively. The size of the domain is $[-2.5; 2.5]^3$. The numerical computation is performed on a 256^3 mesh. Four snapshots are shown on Fig. 3. The interactions of the bow shocks give rise to complicated flow structures in the wake of the spheres.

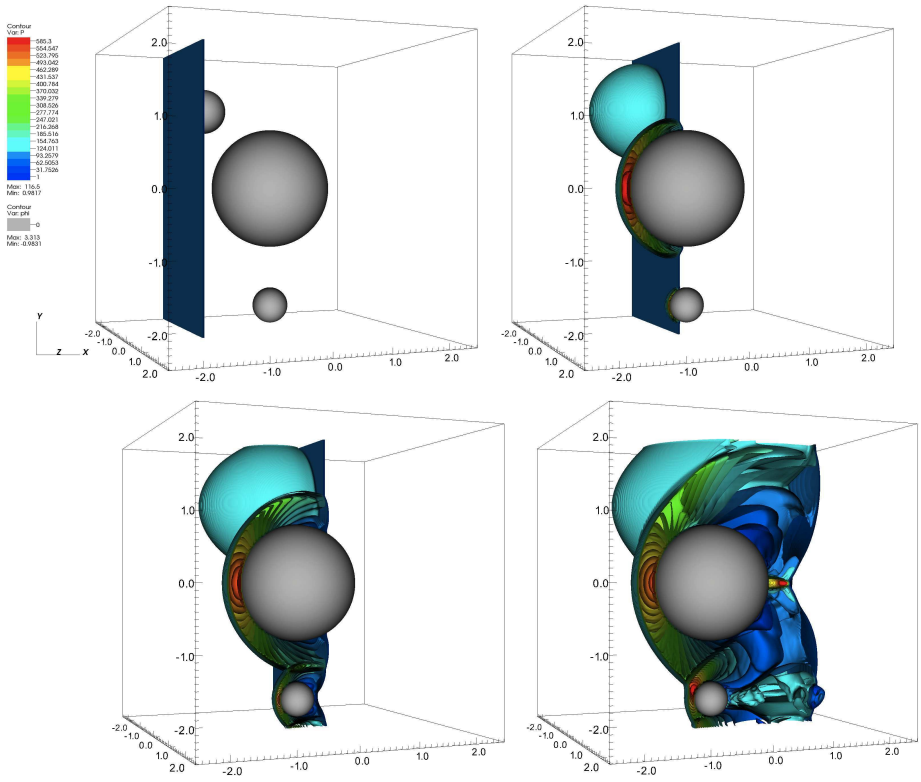

Figure 3: Mach 10 planar shock reflecting on a 3D sphere. 20 isopressure surfaces.

REFERENCES

[1] Coirier W. J. and Powell K. G. An accuracy assessment of cartesian mesh approaches for the Euler equations *J. Comput. Phys.* 1995 **117** 121–131

[3] A. Dadone and B. Grossman Ghost-cell method for analysis of inviscid three dimensionnal flows on cartesian grids *Computers and Fluids* 2007 **36** 1513–1528

[4] Y. Gorsse, A. Iollo, H. Telib, L. Weynans A simple second order cartesian scheme for compressible Euler flows *J. Comput. Phys.* 2012 **231** 7780-7794